The *Dictyostelium* type V myosin MyoJ is responsible for the cortical association and motility of contractile vacuole membranes

Goeh Jung,[1] Margaret A. Titus,[2] and John A. Hammer III[1]

[1]Laboratory of Cell Biology, National Heart, Lung, and Blood Institute, National Institutes of Health, Bethesda, MD 20892
[2]Department of Genetics, Cell Biology, and Development, University of Minnesota, Minneapolis, MN 55455

The contractile vacuole (CV) complex in *Dictyostelium* is a tubulovesicular osmoregulatory organelle that exhibits extensive motility along the actin-rich cortex, providing a useful model for investigating myosin-dependent membrane transport. Here, we show that the type V myosin myoJ localizes to CV membranes and is required for efficient osmoregulation, the normal accumulation of CV membranes in the cortex, and the conversion of collapsed bladder membranes into outwardly radiating cortical CV tubules. Complementation of myoJ-null cells with a version of myoJ containing a shorter lever arm causes these radiating tubules to move at a slower speed, confirming myoJ's role in translocating CV membranes along the cortex. MyoJ-null cells also exhibit a dramatic concentration of CV membranes around the microtubule-organizing center. Consistently, we demonstrate that CV membranes also move bi-directionally on microtubules between the cortex and the centrosome. Therefore, myoJ cooperates with plus and minus end–directed microtubule motors to drive the normal distribution and dynamics of the CV complex in *Dictyostelium*.

Introduction

The contractile vacuole (CV) complex is a specialized intracellular membrane compartment that serves as the osmoregulatory organelle in protozoa. In *Dictyostelium*, this compartment is composed of an interconnected network of tubules and cisternae or bladders. These membranes accumulate excess water (e.g., rain water) that has entered the cell by osmosis by pumping protons and most likely bicarbonate into their lumens. The resulting ion gradient draws the excess water out of the cytoplasm and into the CV lumen. The swollen bladders that are thus generated eventually expel this excess water from the cell by forming transient fusion pores with the plasma membrane (for reviews, see Clarke and Heuser, 1997; Gerisch et al., 2002; Heuser, 2006).

Elegant studies using quick-freeze, deep-etch electron microscopy, interference reflection microscopy, and fluorescent dyes (e.g., FM-64) or CV-specific membrane proteins (e.g., GFP-dajumin and GFP-VatM) to visualize CV membrane dynamics in vivo have revealed a number of important aspects about the CV system in *Dictyostelium* (Heuser et al., 1993; Gabriel et al., 1999; Clarke et al., 2002; Heuser, 2006). First, the tubules and bladders that comprise the system are highly dynamic and pleomorphic. Second, tubules and bladders are rapidly interconvertable. Third, CV membranes do not mix with the endosomal/lysosomal membrane system. Fourth, CV membranes do not normally mix with the plasma membrane, indicating that the process of water expulsion involves a "kiss-and-run" event rather than a full fusion event. Emerging from these studies is a working definition of the CV membrane cycle in *Dictyostelium* in which swollen, mature bladders contact/create fusion pores in the plasma membrane, discharge their dilute electrolyte solution from the cell, and then collapse into a tight "knot" of CV membrane at the site of discharge. This "knot" of collapsed bladder membrane then rapidly rearranges into slender tubules that radiate out across the actin-rich cortex. These tubules subsequently fuse with each other and with immature bladders during the filling phase to eventually create new mature bladders. These repetitive cortical events are seen best in time-lapse confocal images of the ventral surface of

Correspondence to John A. Hammer III: hammerj@nhlbi.nih.gov

Abbreviations used in this paper: CV, contractile vacuole; GTD, globular tail domain; MTOC, microtubule-organizing center; NZ, nocodazole; WT, wild type.

This article is distributed under the terms of an Attribution–Noncommercial–Share Alike–No Mirror Sites license for the first six months after the publication date (see http://www.jcb.org/misc/terms.shtml). After six months it is available under a Creative Commons License (Attribution–Noncommercial–Share Alike 3.0 Unported license, as described at http://creativecommons.org/licenses/by-nc-sa/3.0/).

The Rockefeller University Press $30.00
J. Cell Biol. Vol. 186 No. 4 555–570
www.jcb.org/cgi/doi/10.1083/jcb.200810147

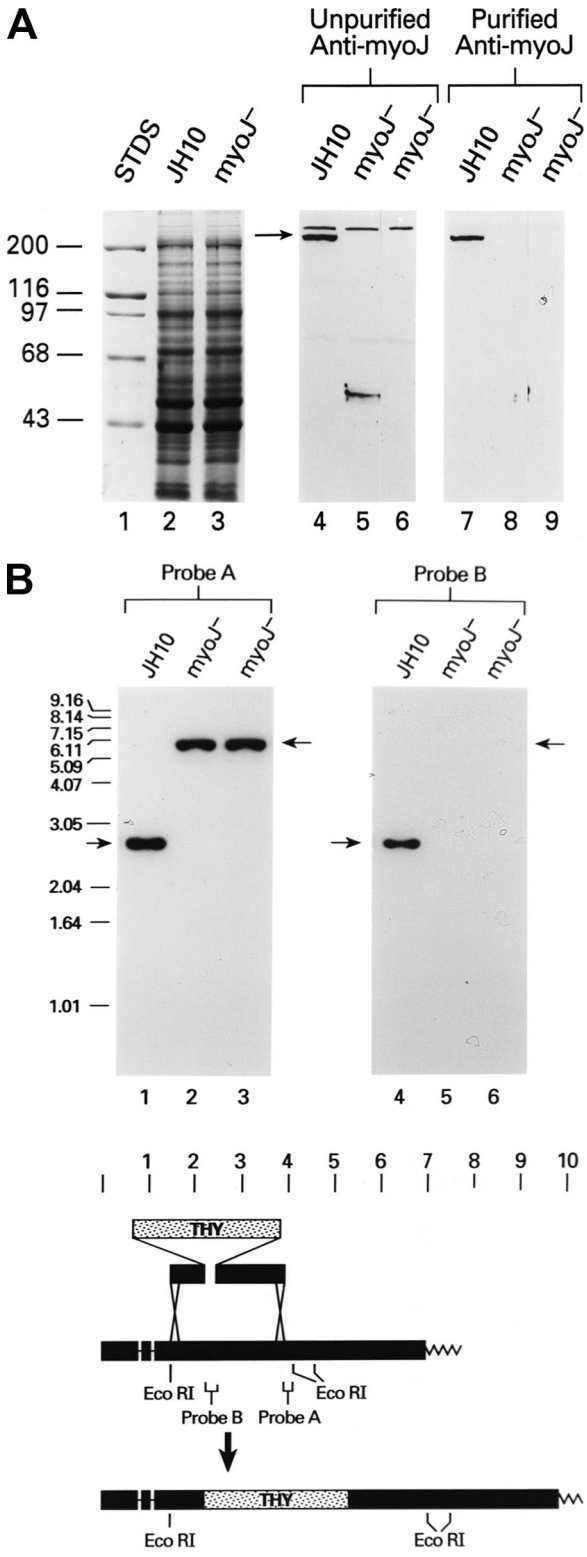

Figure 1. **Generation of a myoJ-specific antibody and creation of myoJ-null cells.** (A) Shown are Coomassie blue–stained gels of whole cell extracts prepared from WT (JH10) cells (lane 2) and one of the myoJ-null cell lines (lane 3), and Western blots performed using extracts from WT cells (lanes 4 and 7) and two independent myoJ-null cell lines (lanes 5, 6, 8, and 9) and probed with either the crude (lanes 4–6) or the purified (lanes 7–9) anti-myoJ antibody. Note that the disruption of the myoJ gene results in the loss of the ∼225-kD band present in WT cell extracts probed with the crude anti-serum (see arrow), which this is the only band present when WT extracts are probed with the purified antibody, and that this band is absent in myoJ-null cell extracts probed with the purified antibody. (B) The schematic at the bottom shows the design of the linear DNA fragment designed to disrupt the myoJ heavy chain gene. This fragment contains two segments of heavy chain coding sequence placed 5′ and 3′ of the THY selectable marker cassette, which confers on JH10 cells the ability to grow in media lacking thymidine. The schematic also shows the predicted change in the size of an internal EcoR1 fragment present within the myoJ chromosomal locus after a double crossover, homologous recombination event involving the linear disruption fragment, as well as the positions of probe A (which should detect the shift in the size of the internal EcoR1 from ∼2.7 kb in WT cells to ∼5.7 kb in knockout cells) and probe B (which, because it corresponds to the gap between the two fragments of myoJ coding sequence used in the disruption fragment, should not recognize the ∼5.7 kb EcoR1 fragment generated in knockout cells). The Southern blots at the top show that all of these predictions hold true when genomic DNAs from JH10 cells (lanes 1 and 4) and two independent myoJ-null cell lines (lanes 2, 3, 5, and 6) are hybridized with probe A (left) and probe B (right) (see arrows).

adherent cells because this configuration places a large area of the plasma membrane and subjacent actin-rich cortex within a single focal plane.

The close association of CV membranes with the actin-rich cortex and the dramatic motility of CV tubules along the cortex have led to the suggestion that CV membranes in *Dictyostelium* recruit one or more myosin motors (Zhu and Clarke, 1992). Here, we show that the *Dictyostelium* type V myosin myoJ (Hammer and Jung, 1996; Peterson et al., 1996) (also referred to as myosin 5b; Kollmar, 2006) is responsible for the steady-state association of CV membranes with the cortex and for the cortical motility of CV tubules that emanate from collapsed bladder membranes after water discharge. We also provide evidence, gleaned in part from analysis of myoJ-null cells, that myoJ cooperates with plus and minus end–directed microtubule motors to drive the proper distribution and function of the CV complex in *Dictyostelium*.

Results

MyoJ localizes to CV complex membranes

To localize endogenous myoJ, we raised a polyclonal antibody against a portion of the central coiled-coil domain of its 225-kD heavy chain. Subtractive purification of the crude antisera (Fig. 1 A, lanes 4–6) against a myoJ-null cell extract yielded a purified antibody that sees a single, 225-kD polypeptide in whole cell extracts of wild-type (WT) cells (Fig. 1 A, lane 7) but not in extracts of myoJ-null cells (Fig. 1 A, lanes 8 and 9). WT cells double stained with this antibody and a monoclonal antibody against the 100-kD subunit of the vacuolar proton pump, a bona fide CV membrane marker (Fok et al., 1993; Liu and Clarke, 1996), showed that the majority of myoJ in fixed cells colocalizes with the proton pump (Fig. 2, A–D). Localization of myoJ on phase-lucent CV bladders was very clear (Fig. 2, black and white arrows). Unequivocal localization of myoJ on CV tubules was hampered by the fact that tubules are poorly preserved in fixed cells, but probably corresponds to the double-stained strands present in between bladders (Fig. 2, white arrowheads). As expected, myoJ-null cells exhibited a negligible signal for myoJ (Fig. 2, E–H).

Interestingly, CV membranes appear highly aggregated in myoJ-null cells (Fig. 2, E–H, and see below). MyoJ also colocalized extensively with calmodulin, a second bona fide CV membrane marker (Zhu and Clarke, 1992) (Fig. 2, I–L). Localization of myoJ on calmodulin-positive CV bladders was very striking. Given that myoJ could possess as many as 12 calmodulin molecules as light chains (as is the case for mouse myosin Va), we sought to determine whether the intense staining of CV membranes for calmodulin was myoJ dependent. Fig. 2 (M–P) shows that the aggregated CV membranes in myoJ-null cells still stain intensely for calmodulin. Although we cannot rigorously exclude the possibility that the amount of calmodulin on CV membranes is diminished to some extent in myoJ-null cells, it clearly does not disappear. We conclude, therefore, that the striking colocalization of calmodulin with CV membranes is not myoJ dependent. Consistently, myoJ does not appear to use calmodulin as a light chain (unpublished data).

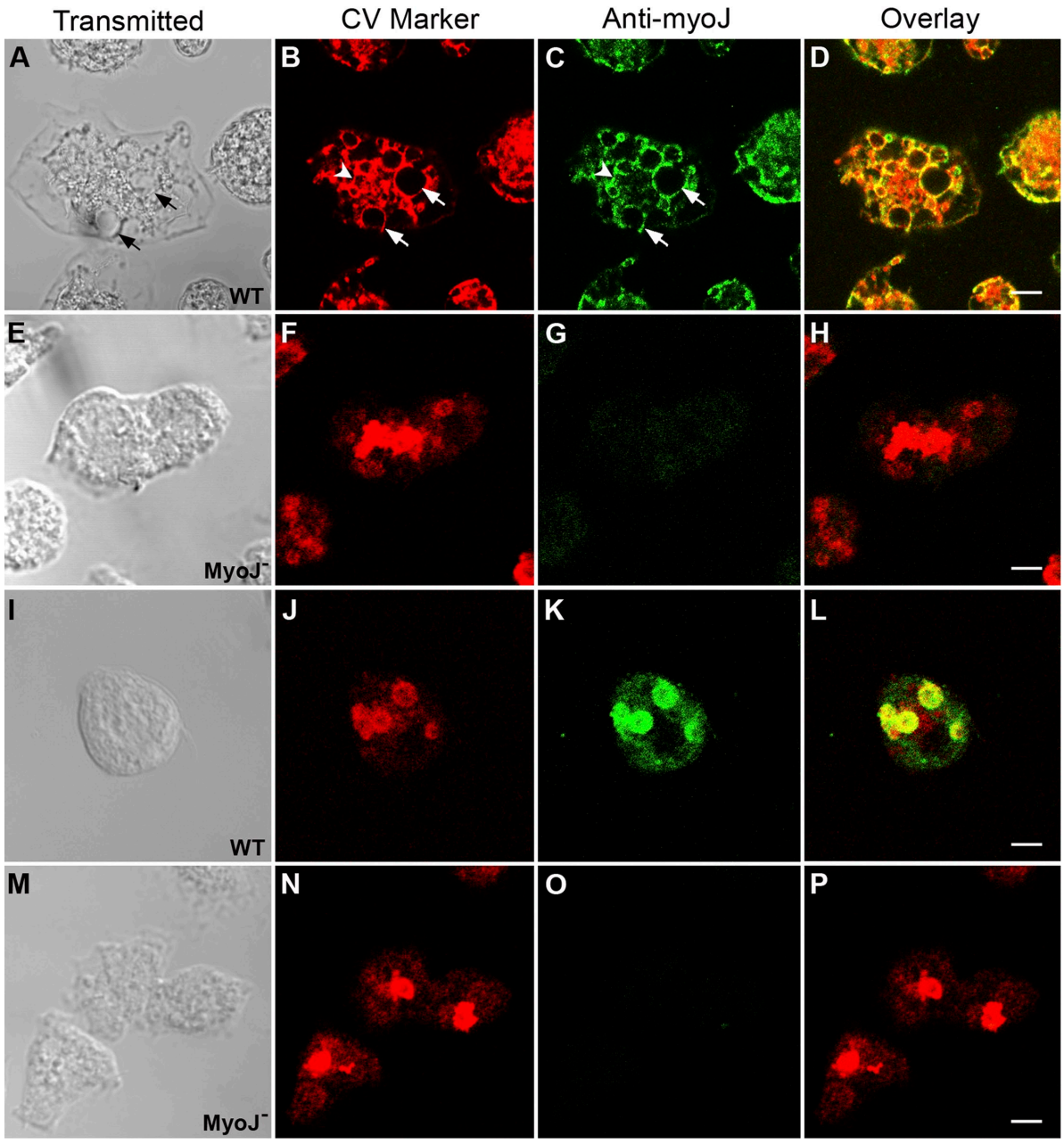

Figure 2. **Endogenous myoJ is concentrated on contractile vacuole membranes.** Shown are wild-type (A–D and I–L) and myoJ-null (E–H and M–P) cells double stained for CV membranes (anti-proton pump in B and F, anti-calmodulin in J and N) and anti-myoJ (purified antibody) (C, G, K, and O). D, H, L, and P show the overlaid images. The black arrows in A, and the corresponding white arrows in B and C, point to phase-lucent CV bladders that are positive for both the proton pump and myoJ. The white arrowheads in B and C point to what may be CV tubules that are positive for both the proton pump and myoJ. We note that although the proton pump stained here is also present in endosomal membranes, its density there is about one tenth that in CV membranes (Gerisch et al., 2002), so at the exposures shown here only CV membranes are visualized. The cells in A–D were overlaid with agar before fixation and imaged in widefield. Bars: 4 μm.

MyoJ-null cells exhibit a defect in CV complex function

To gauge the importance of myoJ in CV complex function, we created myoJ-null cell lines by homologous recombination (Fig. 1 B). The thymidine auxotroph JH10 was transformed with a linear gene disruption fragment designed to insert the thymidine marker into the myoJ heavy chain gene and, at the same time, to delete a portion of the heavy chain coding sequence (Fig. 1 B, bottom schematic). Southern blots showed that ∼20% of transformants exhibited the desired structural rearrangements of the gene: an ∼3-kb increase in the size of the EcoR1 fragment spanning the integration site (seen with Probe A; Fig. 1 B, left), and the removal of a portion of the myoJ coding sequence (seen with Probe B; Fig. 1 B, right). As expected, these transformants are devoid of the 225-kD myoJ heavy chain polypeptide using either the unpurified (Fig. 1 A, lanes 5 and 6) or purified α-myoJ antisera (Fig. 1 A, lanes 8 and 9). All subsequent studies were performed initially with three independent myoJ-null cell lines and in every case the phenotypes were indistinguishable.

To access CV complex function in the absence of myoJ, the viabilities of WT (JH10) and myoJ-null cells were determined by plaque assay at various times after placing the cells in distilled water in order to maximally challenge the CV system. Fig. 3 A shows that although even WT cells are sensitive to extended incubation in water, myoJ-null cells are much more sensitive, exhibiting an approximately twofold greater reduction in the percent of surviving cells after 3 h in water, and an approximately threefold greater reduction after 24 h. We conclude, therefore, that although the CV system must still function to some extent in the absence of myoJ (otherwise all the null cells should die), its function is significantly compromised when myoJ is missing.

MyoJ-null cells exhibit a dramatic redistribution of their CV membranes from the cell cortex to the cell center

To facilitate subsequent analyses of CV complex function in the presence and absence of myoJ, the CV membrane marker GFP-dajumin was stably introduced into WT and myoJ-null cells. This marker decorates both CV bladders and tubules, allowing their distribution and dynamics to be visualized in living cells (Gabriel et al., 1999). As expected, endogenous myoJ colocalizes extensively with CV membranes illuminated by GFP-dajumin (Fig. S1). Live cells expressing GFP-dajumin were routinely imaged at 1 frame per second using a spinning disk confocal microscope under conditions of minimal illumination to avoid inhibition of CV complex function. Fig. 3 (B–E) shows that the distribution of CV membranes is dramatically altered in myoJ-null cells. Fig. 3 C shows a single confocal section along the ventral surface of several WT cells where the organization of CV bladders and interconnecting tubules, which spread across the actin-rich cortex under the plasma membrane, is best viewed. For reasons that will become clear below, Fig. 3 E shows a single confocal section in the middle of several myoJ-null cells, where an abnormal accumulation of CV membranes is seen. This dramatic aggregation of CV membranes near the cell center was seen not only in every myoJ-null cell expressing GFP-dajumin (which for reasons discussed in the figure legend is not 100% despite the fact that the cells are clonal), but also in essentially 100% of null cells in which the organization of the CV complex was determined by fixation and staining with antibodies to either

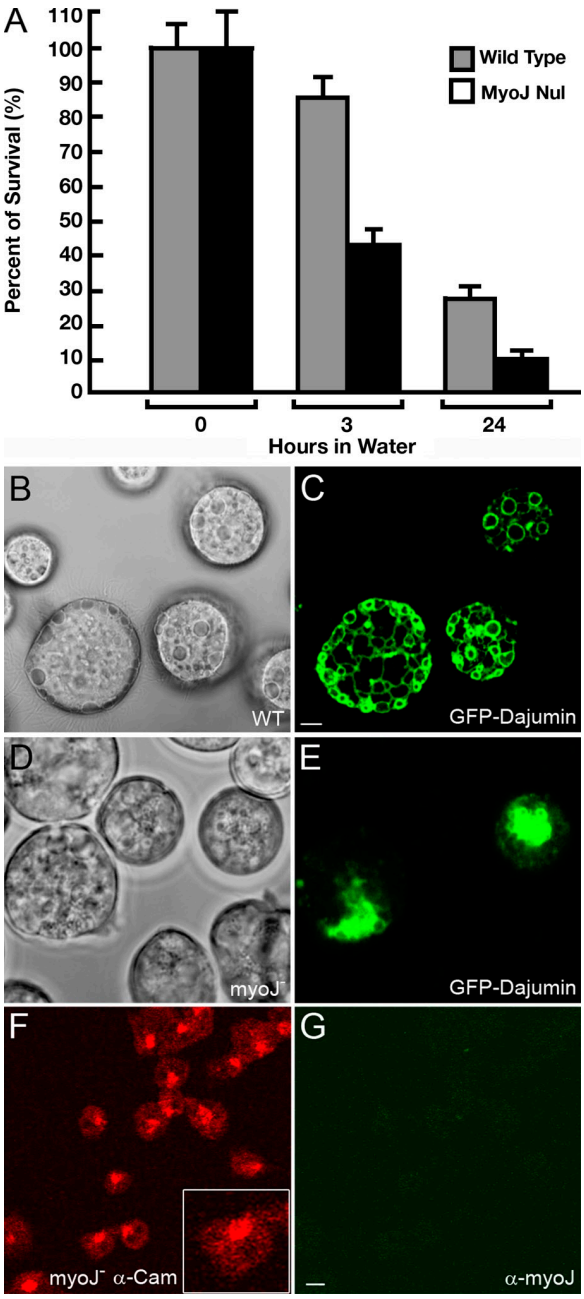

Figure 3. **MyoJ-null cells exhibit impairment in CV function and a dramatic redistribution of their CV membranes.** (A) Percentage of WT and myoJ-null cells that survived exposure to water for 0, 3, and 24 h. For the 0-h measurement, viability was measured immediately after the transfer of cells from growth media to water. The values for WT and mutant cells (n = 3) were significantly different at both 3 h ($P < 0.01$) and 24 h ($P < 0.025$) (Mann-Whitney). (B–E) Transmitted (B and D) and fluorescent (C and E) images of WT (B and C) and myoJ-null cells (D and E) expressing GFP-dajumin. For reasons explained in the text, the image for WT cells is a ventral confocal section, whereas the image for the mutant cells is a confocal section through the center of the cell. As is typical for *Dictyostelium*, although these cells are clonal isolates of stable transformants for GFP-dajumin, the expression of GFP-dajumin is strong in only a subset of cells. (F and G) Field of myoJ-null cells stained for calmodulin and for myoJ, respectively, to demonstrate that CV membranes are aggregated in every mutant cell. Bars: (C and E) 3 µm; (G) 9 µm.

calmodulin (Fig. 3 F) or the proton pump (not depicted) rather than by introduction of GFP-dajumin. Conversely, through-focusing of WT cells, whether expressing GFP-dajumin or fixed and stained for the pump or calmodulin, never showed such a dramatic central accumulation of CV membranes.

To gain further insight into the nature of this defect in CV membrane distribution, WT and myoJ-null cells expressing GFP-dajumin were optically sectioned (Fig. S2). A Z-series of a WT cell (Fig. S2 A) shows that CV membranes normally accumulate not only along the ventral cortex (arrow), but also along the lateral and dorsal cortex (arrowheads). Some degree of central accumulation of CV membranes in middle sections of WT cells is always seen as well. In the best images, these centrally positioned membranes are seen to be connected to bladders at the cortex by tubular connections (Fig. S2 D, arrowheads). The nature and significance of these connections are considered in detail below. In contrast to WT cells, Z-series of myoJ-null cells (Fig. S2 B) show that the majority of them contain a single large aggregate of CV membranes positioned approximately in the middle of the cell (arrow). Strikingly, CV membranes are almost always absent from the ventral, lateral, and dorsal cortices of null cells. Indeed, the presence of the single CV bladder along the ventral surface of the null cell shown (arrowhead) is one of the rare instances in which we could find any CV membrane at the ventral cortex of a null cell. In sharp contrast, WT cells always exhibit extensive accumulations of CV membranes at their ventral surface.

To extend these observations, we imaged the dynamics of CV membranes at the ventral surface of WT and null cells expressing GFP-dajumin (Fig. 4 and Video 1). WT cells (Fig. 4, A1–A8; Video 1, left movie) exhibited the same dramatic dynamics described previously (Gabriel et al., 1999), with tubules and bladders moving, fusing, and rapidly changing shape. Most interestingly (Fig. 4, see boxed region), when a mature bladder expels water (Fig. 4, A1–A4), its limiting membrane collapses into a bright knot or rosette (Fig. 4, A5 and A6), as described previously (Gabriel et al., 1999), which then rapidly converts into tubules that grow out from the knot, spreading across the actin-rich cortex (Fig. 4, A7 and A8; Video 1, left movie). Extensive efforts to find similar images in null cells were completely futile. In those relatively rare instances where a CV bladder was found at the ventral surface (Fig. 4, B1–B8; Video 1, right movie), it was usually nonmotile and often did not undergo discharge during two minutes of imaging. Together, these observations indicate that the steady-state accumulation of CV membranes in the actin-rich cortex is myoJ dependent.

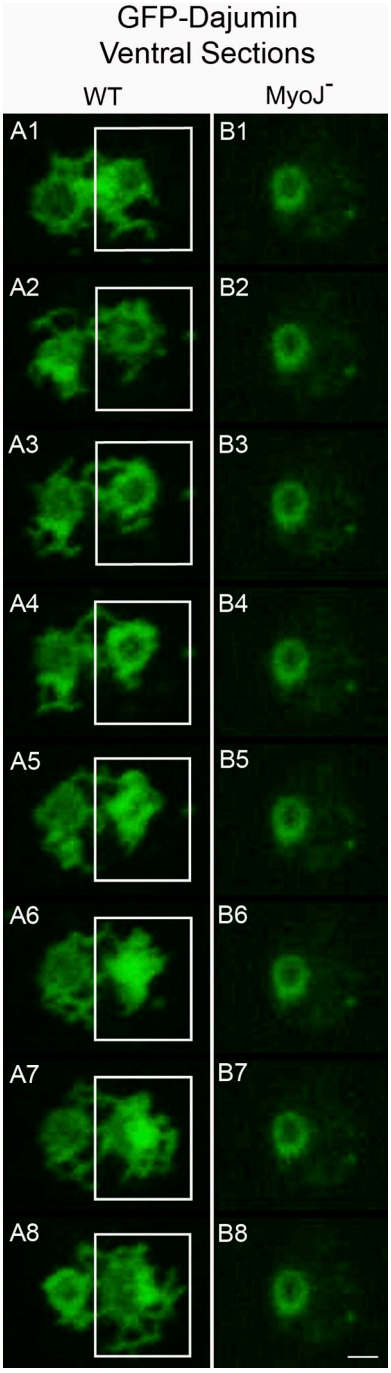

Figure 4. **The normal ventral accumulation of CV membranes and the typical dynamics exhibited by these membranes are absent in myoJ-null cells.** Shown are individual frames from the two movies in Video 1 that demonstrate the typical behavior of CV membranes in the ventral cortex of a WT cell (A1–A8) and a myoJ-null cell (B1–B8). The boxed area in A1–A8 highlights for a single CV bladder the events that comprise most of the CV cycle. Bar: (B8) 2 μm.

CV membranes congregate at the MTOC in myoJ-null cells

To begin to address the mechanism responsible for the aggregation of CV membranes in myoJ-null cells, we stained WT and null cells expressing GFP-dajumin for α-tubulin (Fig. 5). In WT cells (Fig. 5, A–C), CV membranes, like the interphase microtubule array, are spread throughout the cell. In myoJ-null cells (Fig. 5, D–F), on the other hand, CV membranes are aggregated in the presence of a normal-looking microtubule array. More importantly, in almost every null cell examined, this aggregate is roughly centered where the minus ends of the microtubules converge at the microtubule-organizing center (MTOC), suggesting that CV membranes accumulate at the minus end of microtubules in cells without myoJ. Two additional observations supported this conclusion. First, staining null cells for γ-tubulin to visualize the centrosome (Fig. 5, G–J) showed that the CV membrane aggregate overlaid this structure or was immediately adjacent to it. This was seen in 83% of null cells ($n = 200$). Therefore, although

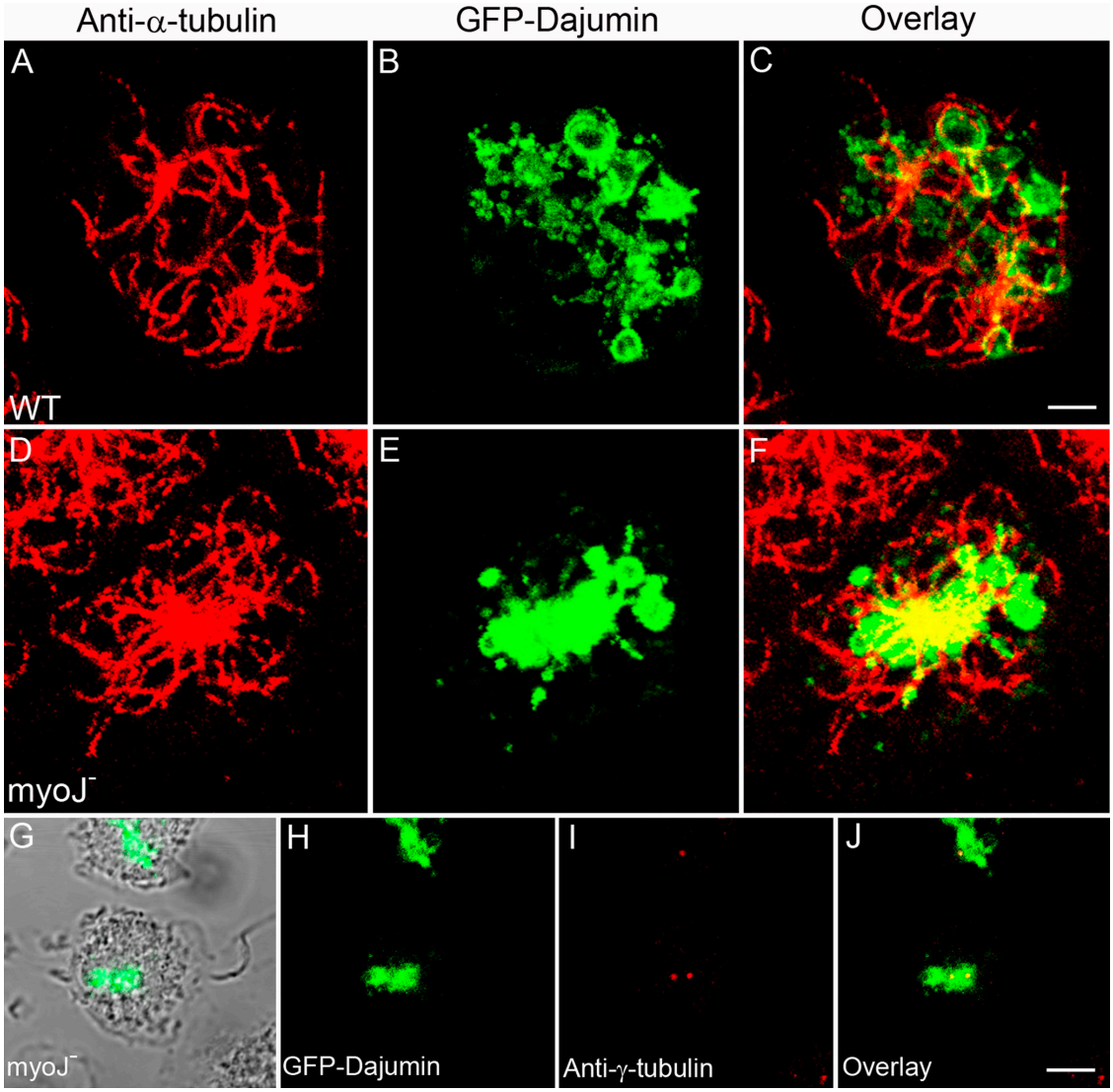

Figure 5. **The central aggregate of CV membranes in myoJ-null cells is focused at the MTOC.** Shown are a WT cell (A–C) and a myoJ-null cell (D–F) that were expressing GFP-dajumin (B and E) and that were agar overlaid and stained for α-tubulin (A and D). (C and F) Corresponding overlaid image. Also shown are two myoJ-null cells (G) that were expressing GFP-dajumin (H) and that were stained for γ-tubulin (I). J shows the overlaid image. The cell in the middle of the image has two closely spaced centrosomes. Bars: (C and E) 3 µm; (J) 5 µm.

this aggregate assumes a variety of positions in the XY dimensions in both fixed and living cells (e.g., both dead center and on the cell edge), it almost always goes together with the MTOC. Second, imaging of CV membrane dynamics in living cells (see below) showed that the CV membrane aggregate in null cells, and a much smaller steady-state accumulation of CV membranes seen in the center of WT cells, is always immediately adjacent to the nucleus and focused at a single spot. Both of these characteristics are consistent with the position of the centrosome.

CV tubules and vesicles move bi-directionally on microtubules between the cortex and the MTOC

As discussed above, CV membrane dynamics in living *Dictyostelium* have previously been imaged almost exclusively at the ventral surface of adherent cells because this configuration places a large area of the plasma membrane and subjacent actin-rich cortex within a single focal plane. These images have revealed in dramatic fashion the conversion of collapsed bladder membranes into tubules that radiate out across the actin-rich cortex after water expulsion (Gabriel et al., 1999; Fig. 4, A1–A8; Video 1). The large accumulation of CV membranes we observed around the MTOC in the center of myoJ-null cells, together with the consistent presence of a small amount of CV membranes at the MTOC in WT cells, and the presence of tubular connections between these centrally located membranes and CV membranes at the cortex in the cell periphery (Fig. S2 D), led us to visualize CV membrane dynamics in the middle of the cell. We began by examining WT cells expressing GFP-dajumin.

Fig. 6 and Video 2 show images of three typical WT cells where GFP-dajumin was imaged in the middle of the cell. Together, these cells exhibit the full range of normal CV membrane movements that we observed in this optical plane. First, when mature bladders at the cortex collapse after water expulsion,

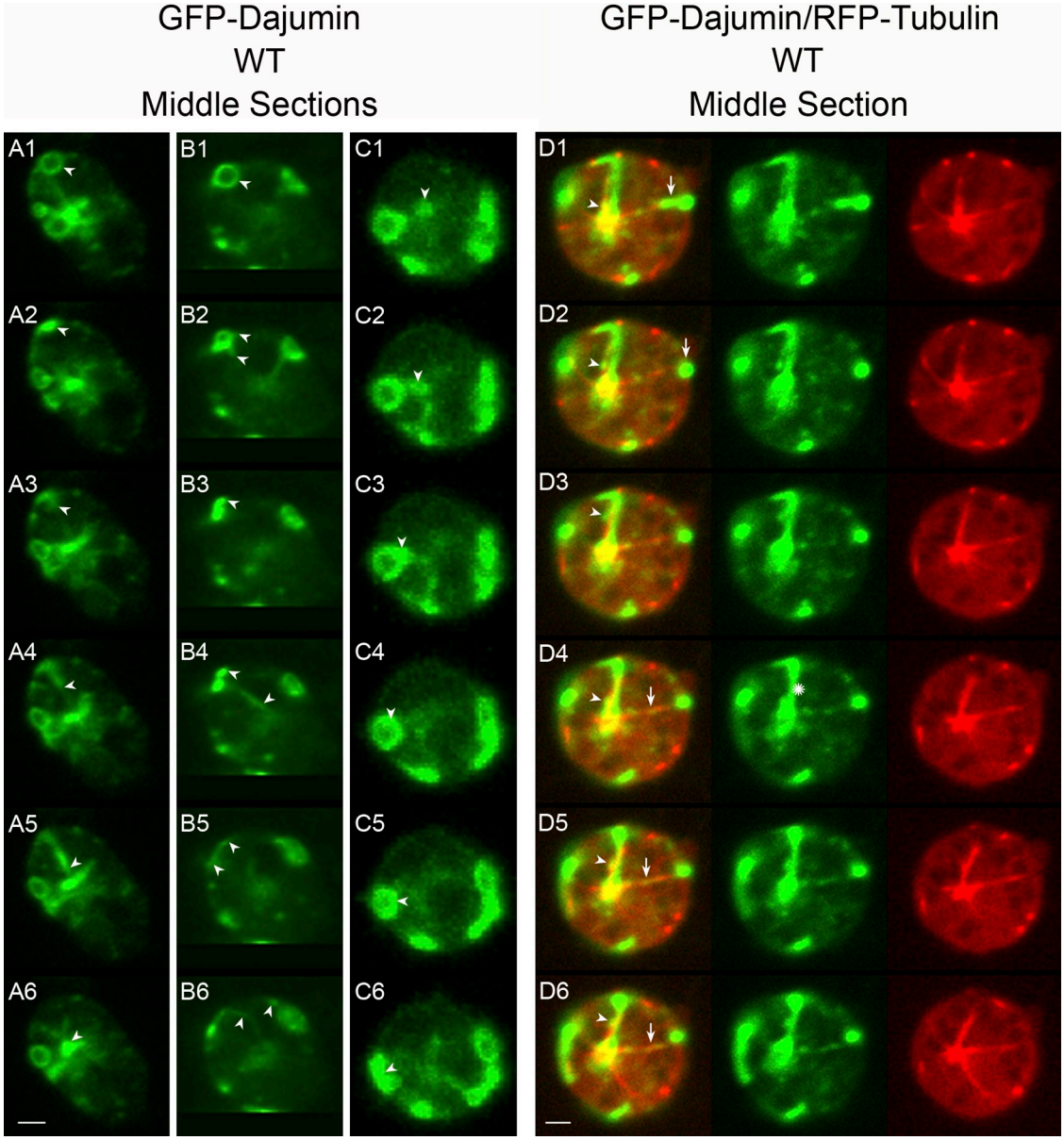

Figure 6. **CV membranes move bidirectionally on microtubules between the cortex and the MTOC.** Shown in A1–A6, B1–B6, and C1–C6 are individual frames from the three movies presented in Video 2 that demonstrate the typical, bidirectional, microtubule-dependent movements of CV membranes that occur between the cortex and the centrosome in WT cells. D1–D6 show individual frames from Video 4 that demonstrates the movement of CV membranes along microtubules in cells simultaneously expressing GFP-dajumin and RFP-tubulin. The meanings of the arrows/arrowheads are described in the text (the asterisk in D4 marks a stable tubular connection between the MTOC and the cortex). Bars: (A6 and D6) 2 μm.

some portion of their membrane typically moves inward along a curvilinear path to join the small steady-state cluster of CV membrane at the MTOC. In the case of the cell shown in Fig. 6, A1–A6 (Video 2, left movie), the entire remnant of the collapsed bladder appears to move inward to the MTOC (follow the arrowheads). In the case of the cell shown in Fig. 6, B1–B6 (Video 2, center movie), a portion of the collapsed bladder membrane moves inward to the MTOC (B2–B4) while the rest appears to spread out along the cortex (Fig. 6, B4–B6; follow the arrowheads). Second, both tubular and vesicular CV structures constantly emanate from the central cluster of CV membranes and move in a curvilinear path out to the cortex, where they usually fuse with CV membranes already present there. In many cases, the resulting expansion of the peripheral membrane structure results in the rapid formation of a mature bladder, followed shortly thereafter by water expulsion. All of these events are demonstrated by the WT cell in Fig. 6, C1–C6 (Video 2, right movie), where a CV vesicle present in the center of the cell (C1) can be seen to move to the cortex (C1–C4) and fuse with a preexisting cortical CV bladder, triggering bladder collapse (C4–C6; follow the arrowheads). Layered over top of these bidirectional, tubulovesicular movements are more stable tubular connections between central and cortical CV membranes. These are evident in the cells depicted in Video 2, in the optical sections in Fig. S2 D, and in the single, central confocal section through a field of WT cells shown in Video 3, which reveals

such connections in essentially every dajumin-expressing cell, giving them a star-like appearance.

Several observations indicate that these bi-directional CV membrane movements are microtubule based. First, their paths are always curvilinear and their central origin or destination is always a single spot adjacent to the nucleus (i.e., the MTOC). Second, they are both fast (1.35 ± 0.56 µm/s [$n = 91$] and 1.19 ± 0.79 µm/s [$n = 79$] for centripetal and centrifugal events, respectively) and persistent. Third, CV tubules can be seen to align with microtubules in fixed cells stained for α-tubulin (unpublished data). Fourth, the movements are sensitive to nocodazole (see below). Finally, time-lapse imaging of WT cells expressing both GFP-dajumin and RFP–α-tubulin (Fig. 6, D1–D6; Video 4) demonstrates directly that CV membranes move along microtubules. Specifically, the microtubule-dependent CV membrane movements evident in this cell include the tail end of a tubule movement to the cortex (Fig. 6, arrows in D1 and D2), the sequential movement of two small CV structures (Fig. 6, arrowheads in D1–D3 and D4–D6, respectively), and the movement of CV membranes along the length of a microtubule (Fig. 6, arrows in D4–D6).

CV membranes in myoJ-null cells search the cortex on microtubules but are not captured there

We next imaged CV membrane dynamics in the middle of myoJ-null cells. Fig. 7 (A1–A6) and Video 5 (left movie) show the typical CV membrane movements we observed in this optical plane. Specifically, CV tubules are seen to emanate repeatedly from the central mass of CV membranes, move along curvilinear paths to the cortex, pause, and then return (Fig. 7, follow the arrowheads). Imaging of null cells expressing both GFP-dajumin and RFP-tubulin confirm that these tubular excursions occur on microtubules (Video 6). Therefore, the bi-directional, microtubule-dependent CV membrane movements that normally occur between the MTOC and cortex persist in the absence of myoJ, but cannot on their own generate the stable association of these membranes with the cortex that is seen in WT cells.

WT cells treated with cytochalasin phenocopy myoJ-null cells

MyoJ presumably cooperates with actin to drive the normal accumulation of CV membranes in the cortex. To test this assumption, we treated WT cells with cytochalasin A under conditions where cortical F-actin is essentially depleted. Fig. 8 (A and B) shows that this treatment generates a phenotype similar to that of myoJ-null cells, with GFP-dajumin-positive CV membranes accumulated in the middle of the cell. This central accumulation of membranes at the MTOC, as well as the extensive depletion of CV membranes from the ventral, lateral, and dorsal cortex, was confirmed by optical sectioning (Fig. S2 C) and by comparing the distributions of CV membranes to that of the interphase microtubule array (Fig. 8, C–E). Moreover, as in myoJ-null cells, time-lapse imaging revealed that CV tubules continuously emanate from the central mass of CV membranes in cytochalasin-treated WT cells, move along curvilinear paths to the cortex, pause, and then return (Fig. 7, B1–B6 [follow arrowheads]; Video 5, center movie). Therefore, the steady-state accumulation of CV membranes in the cortex requires both actin and myoJ, presumably in the form of an acto–myoJ complex.

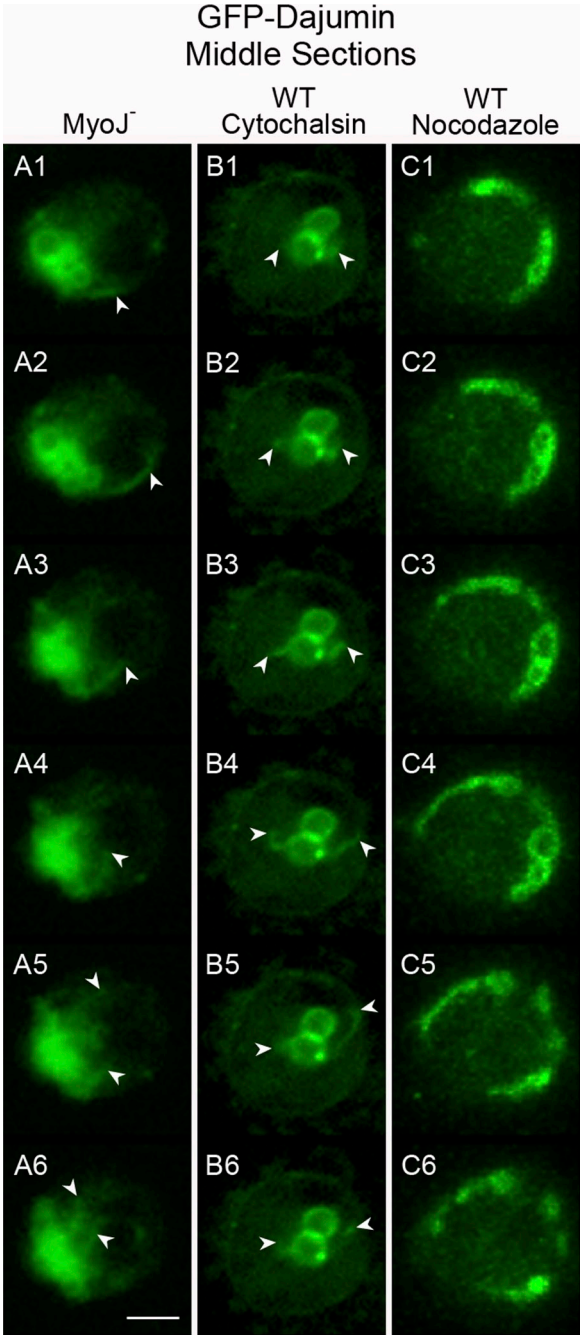

Figure 7. **CV membrane dynamics in myoJ-null cells and in WT cells depleted of either F-actin or microtubules.** Shown are individual frames from the three movies presented in Video 5 that demonstrate the typical behavior of CV membranes in myoJ-null cells (A1–A6), WT cells treated with cytochalasin (B1–B6), and WT cells treated with NZ (C1–C6). The meanings of the arrowheads are described in the text (note that the top arrowhead in A5 and A6 points out an additional CV tubule emanating from the central mass of CV membranes). Although not apparent in B1–B6, the continued incubation of WT cells in the presence of cytochalasin results in the progressive accumulation of GFP-dajumin in the plasma membrane, due presumably to a shift from kiss-and-run to full membrane fusion during bladder discharge events (Heuser, 2006). Bar: (A6) 4 µm.

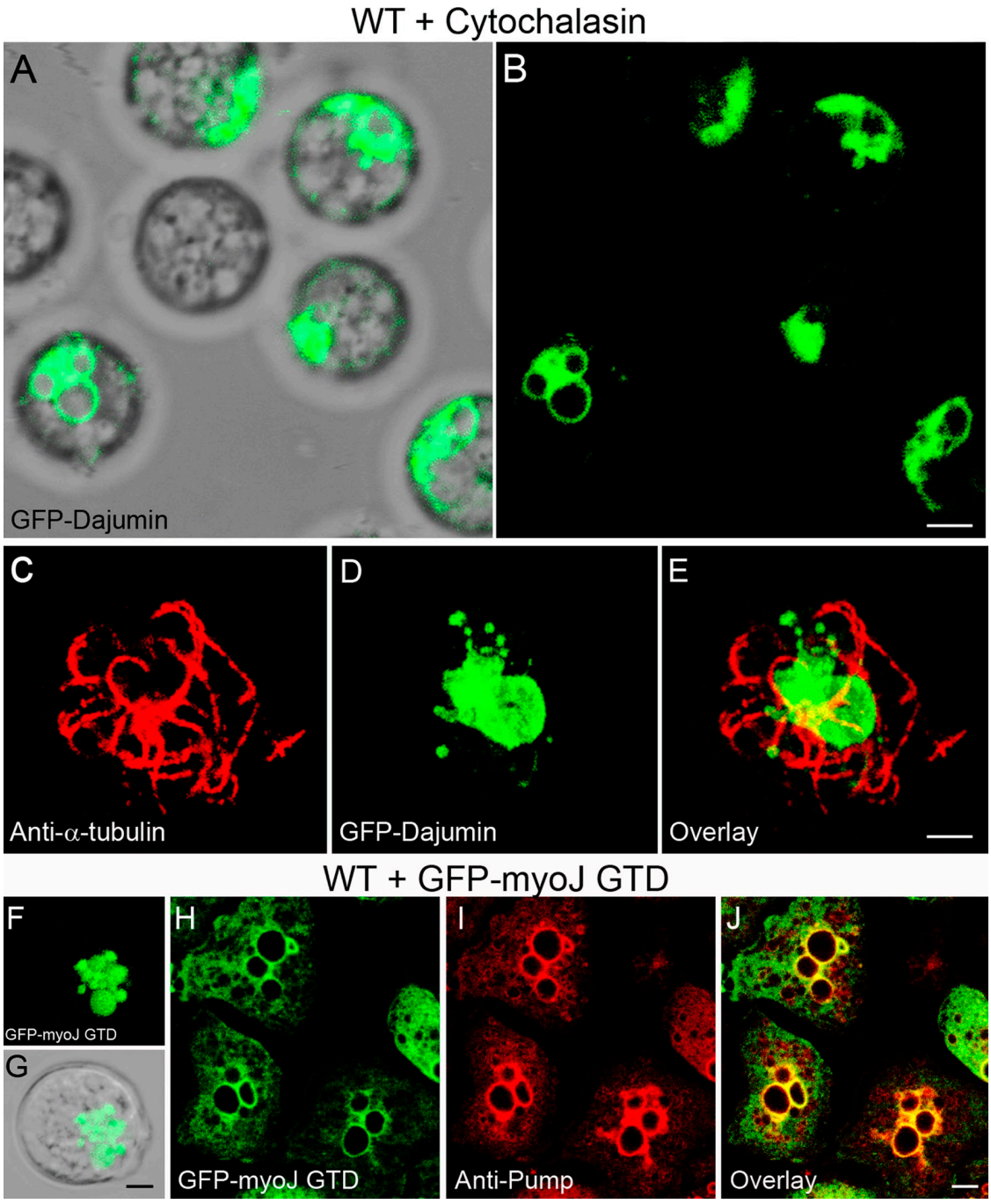

Figure 8. **WT cells depleted of F-actin or overexpressing myoJ's cargo-binding globular tail domain exhibit the same defect in CV membrane distribution as do myoJ-null cells.** Shown are a transmitted/overlaid image (A) and the corresponding fluorescence image (B) of a field of WT cells expressing GFP-dajumin that were incubated for 20 min with 10 μM cytochalasin A. C–E show a cytochalasin-treated cell expressing GFP-dajumin (D) that was stained for microtubules (C) (E; overlaid image). F and G show a fluorescent image of a WT cell expressing GFP-myoJ GTD (F) and the corresponding transmitted/overlaid image (G). H–J show several WT cells that were expressing GFP-myoJ-GTD (H) and that were agar overlaid, fixed, and stained with the anti-proton pump antibody (I) (J; overlaid image). Bars: (B) 5 μm; (E) 4 μm; (G and J) 3 μm.

WT cells expressing the myoJ globular tail domain exhibit the myoJ-null cell phenotype

In numerous contexts, the expression in WT cells of the myosin V globular tail domain (GTD), which contains some or all of the myosin's cargo-specific targeting determinants, has been shown to generate a null cell phenotype via a dominant-negative mechanism (Wu et al., 1998). Fig. 8 (F and G) shows that WT cells expressing myoJs GTD tagged with GFP exhibit a strong central accumulation of GFP-positive membranes, which we confirmed by optical sectioning (not depicted). Staining of these cells with the antibody to the proton pump shows that these central, GFP-GTD–positive membranes are indeed CV membranes (Fig. 8, H–J). This dominant-negative phenotype was seen in 94% ($n = 50$) of GFP-GTD transformants exhibiting obvious GFP fluorescence (which represent ~80% of the cells in clonal lines), but in only 6% of those cells exhibiting no obvious GFP fluorescence

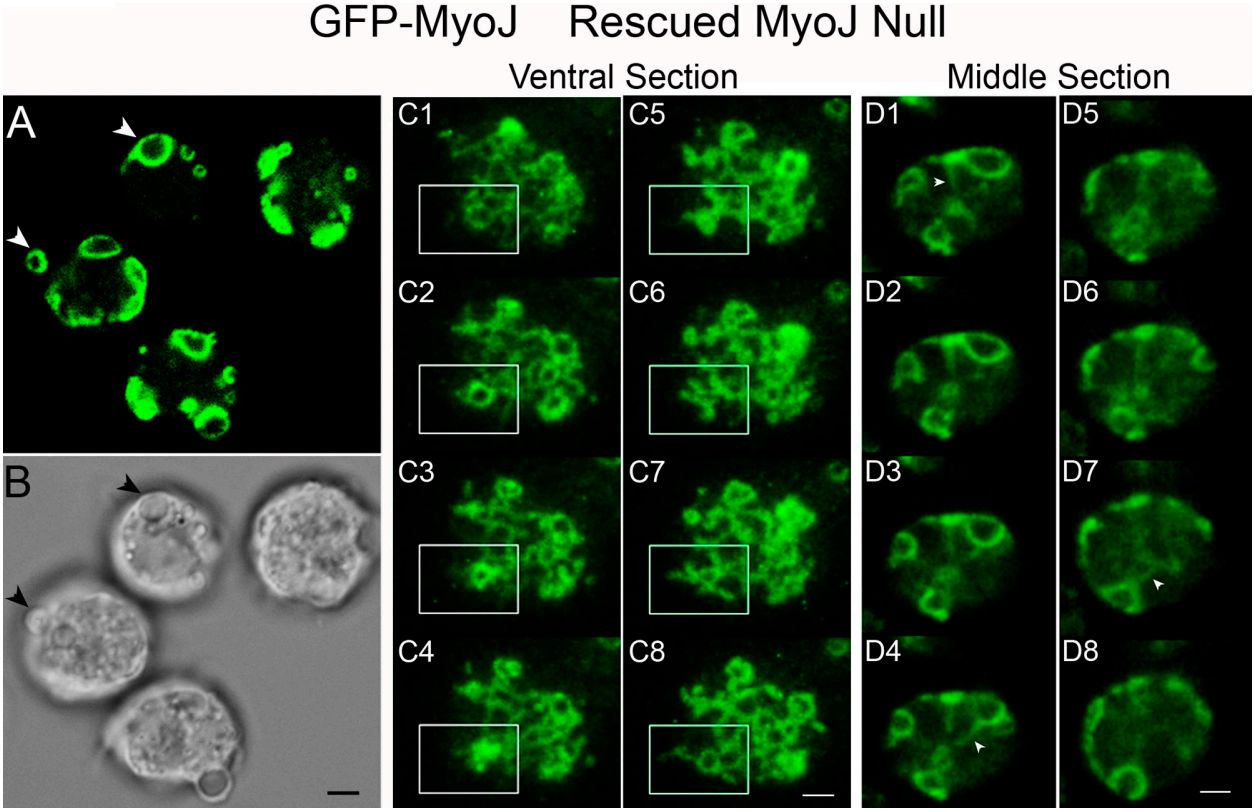

Figure 9. **Expression of full-length, GFP-tagged myoJ in myoJ-null cells rescues all of the defects seen in these cells.** Shown is a fluorescence image (A) of four myoJ-null cells that are expressing GFP-tagged myoJ, and the corresponding transmitted image (B). Also shown are individual frames from the two movies in Video 7 that demonstrate the typical behavior of CV membranes (visualized here by their association with the GFP tagged myosin) in the ventral cortex of a rescued cell (C1–C8) and in the center of a rescued cell (D1–D8). The boxed area in C1–C8 highlights the maturation, discharge, and subsequent radial tubulation of a CV bladder in this rescued cell. Bars: (B) 4 µm; (C8 and D8) 2 µm.

($n = 50$). Moreover, the percent of total GFP-GTD transformants that survived incubation in water for 3 h (67 ± 7.2%; $n = 3$) was significantly lower than for WT cells (85 ± 5.5%; $n = 3$) ($P < 0.025$). Finally, the percentage of dim GFP-GTD transformants increased from 18% at 0 h to 54% after 3 h in water ($n = 1$), indicating that highly expressing cells die preferentially, consistent with a dominant-negative mechanism. Together, these results provide independent confirmation of the myoJ-null cell phenotype and indicate that the sequence in myoJ responsible for its association with CV membranes resides within its GTD.

WT cells treated with nocodazole exhibit a myoJ-dependent hyper accumulation of CV membranes in the cortex

Elimination of the bi-directional, microtubule-dependent movement of CV membranes between the cortex and MTOC would be predicted to restrict CV membranes largely to the cortex in WT cells. To test this prediction, WT cells expressing GFP-dajumin were treated with nocodazole (NZ) under conditions that control experiments show result in a uniform and large reduction in the size of the interphase microtubule array (Fig. S3). Fig. S4 (A–F) and Z-series confocal sections (not depicted) show that CV membranes in these cells become redistributed primarily to the cortex of the cell, and phalloidin staining shows that these membranes overlap with F-actin in the cortex. Images of CV dynamics in the middle of NZ-treated WT cells (Fig. 7, C1–C6; Video 5, right movie) demonstrate that CV membranes now move primarily in the plane of the cortex, and that the bi-directional, microtubule-dependent movements between the cortex and MTOC are almost entirely eliminated.

Given the apparent requirement for myoJ for the stable association of CV membranes with the actin-rich cortex, we reasoned that myoJ-null cells treated with NZ should not show the dramatic cortical association of CV membranes exhibited by WT cells depleted of microtubules. Fig. S4 (G–L) shows that this is the case. Specifically, NZ-treated myoJ-null cells exhibit a cluster of CV membranes that on occasion is associated with small remnants of the microtubule array at the MTOC, but that does not adhere tightly to actin in the cortex, instead being positioned just inside the phalloidin-stained actin-rich cortex.

Full-length, GFP-tagged myoJ targets dramatically to CV membranes and rescues the defects in CV membrane distribution and dynamics in myoJ-null cells

To verify that myoJ targets to CV membranes and that its absence is solely responsible for the null cell phenotypes described above, we sought to rescue null cells with full-length, WT myoJ. To extend the usefulness of this approach, we tagged the myoJ heavy chain with GFP at its N terminus, a location that for vertebrate myosin V does not compromise targeting or function (Wu et al., 2002). Fig. 9 (A and B) shows that GFP-tagged myoJ

targets dramatically to phase-lucent bladders when introduced into myoJ-null cells (see arrowheads). Staining these cells with the proton pump antibody confirmed that these GFP-myoJ–positive membranes are indeed CV membranes, and Z-series confocal images show that CV membranes no longer congregate at the MTOC in these cells, instead being distributed normally to the ventral, lateral, and dorsal cortices (unpublished data). Most dramatically, time-lapse images of the ventral surface of rescued cells show that CV tubules and bladders, which in this case are now visible due to their association with GFP-tagged myoJ (rather than by the presence of GFP-dajumin, as in all preceding time-lapse images), have returned to the ventral cortex in force and display normal dynamics (Fig. 9, C1–C8; note within the boxed region the normal conversion of the bladder membrane to radiating tubules after its collapse in frame C4; Video 7, left movie). Similarly, time-lapse images of central regions of rescued cells show typical, microtubule-dependent, bi-directional movements of CV tubules and vesicles between the cortex and MTOC (Fig. 9, D1–D8; note arrowheads; Video 7, right movie). Finally, the rate of translocation of CV tubules on cortical actin after bladder collapse in rescued myoJ-null cells, as measured by following the displacement over time of the leading tip of GFP-myoJ–labeled tubules (0.51 ± 0.1 μm/s [n = 23]), was indistinguishable from the rate of translocation in WT cells, as measured by following the movement of the tip of GFP-dajumin–labeled tubules (0.48 ± 0.08 μm/sec [n = 24]) (Fig. 10 D). Together, these results confirm that myoJ targets to CV membranes (both tubules and bladders) and that the defects in CV membrane distribution and dynamics in myoJ-null cells are likely due solely to the absence of this myosin.

Collapsed bladder membranes do not undergo the normal conversion to radiating tubules in myoJ-null cells

The results above suggest that, in addition to myoJ's clear role in driving the steady-state association of CV membranes with the actin-rich cortex, it might also be the motor responsible for the movement of CV tubules along cortical actin filaments. These movements are most dramatic after the collapse of mature bladders, at which point the condensed CV membrane usually converts rapidly into tubules that radiate out from the point of collapse. The difficulty in using myoJ-null cells to determine whether these movements are myoJ-dependent is that without myoJ, the ventral surface, which is the only place where these movements can be clearly visualized, rarely contains CV membranes. To help with this problem, we flattened null cells expressing GFP-dajumin by plating them on poly-lysine–coated glass, thereby forcing CV membranes down to the ventral surface (note that we used a much lower concentration of poly-lysine than did Heuser [2006] so as to avoid the catastrophic CV collapse [i.e., full fusion rather than kiss-and-run] he observed on highly adhesive surfaces). Time-lapse images at the ventral surface of these cells reveal that when mature bladders collapse, they no longer transform into radiating tubules in the plane of the membrane (Fig. 10, A1–A8; note the absence of spreading tubules after the collapse of the bladder in frame A5; Video 8, left movie). This was seen in all 22 events we observed in null cells flattened using poly-lysine, as well as in all 5 events we observed without using poly-lysine. Moreover, in most cases the condensed bladder simply refills at the same spot (Fig. 10, A1–A8; note that after the collapse of the bladder in frame A5, it begins refilling at the same spot in frames A6–A8; Video 8, left movie). These results provide strong support for the idea that myoJ powers the extension and radiating movement of CV tubules along actin filaments in the cell cortex.

Complementation of myoJ-null cells with GFP-myoJ containing a mutation predicted to dramatically slow the myosin restores the cortical association of CV membranes, but not the conversion of collapsed bladders to radiating tubules

If myoJ drives the movement of CV tubules emanating from collapsed bladders, complementation of myoJ-null cells with versions of myoJ exhibiting altered mechanochemical properties should result in corresponding changes in the dynamics of these CV membrane tubules. To test this, we initially complemented myoJ-null cells using FL-GFP–tagged myoJ containing the point mutation G488A, which in chicken myosin Va (G440A) slows the myosin's actin-activated ATPase by ∼400-fold, trapping the myosin in an ATP-bound form that has a relatively high affinity for F-actin (apparent actin affinity ∼0.2 μM) (Yengo et al., 2002). If this mutation has the same effect on myoJ, it should cause myoJ to bind F-actin very readily in vivo (where the ATP concentration is high) but to step extremely slowly. Imaging the ventral surface of myoJ-null cells complemented with GFP-myoJ-G488A showed that the association of CV membranes with the cortex was largely restored, as all 30 cells examined contained two or more CV bladders attached to the ventral surface (Fig. 10, B1–B8). When these bladders underwent discharge, however, their conversion to radiating tubules was not observed (Fig. 10, B1–B8; note that the bladder marked by the arrowhead in frame B1 does not undergo obvious conversion to radiating tubules after its collapse in frame B5, but instead refills at the same spot in frames B7 and B8; Video 8, center movie). Our interpretation of these results is that the relatively high affinity we assume GFP-myoJ-G488A has for F-actin in vivo, combined with its ability to bind to CV membranes through its GTD, is sufficient to allow the mutated myosin to recruit CV membranes to cortical actin, but that its very slow ATPase is not sufficient to allow it to drive the extension and radiating movement of CV tubules after bladder collapse.

Complementation of myoJ-null cells with GFP-myoJ containing a shorter lever arm restores both the cortical association of CV membranes and the extension of CV membrane tubules, but the tubules move at half their normal speed

Perhaps the most convincing argument to date that a particular myosin moves a particular organelle comes from the work of Schott et al. (2002) on the yeast type V myosin myo2p, where the speed of secretory vesicles moved by myo2p was shown to slow progressively as *Myo2*-null cells were complemented with

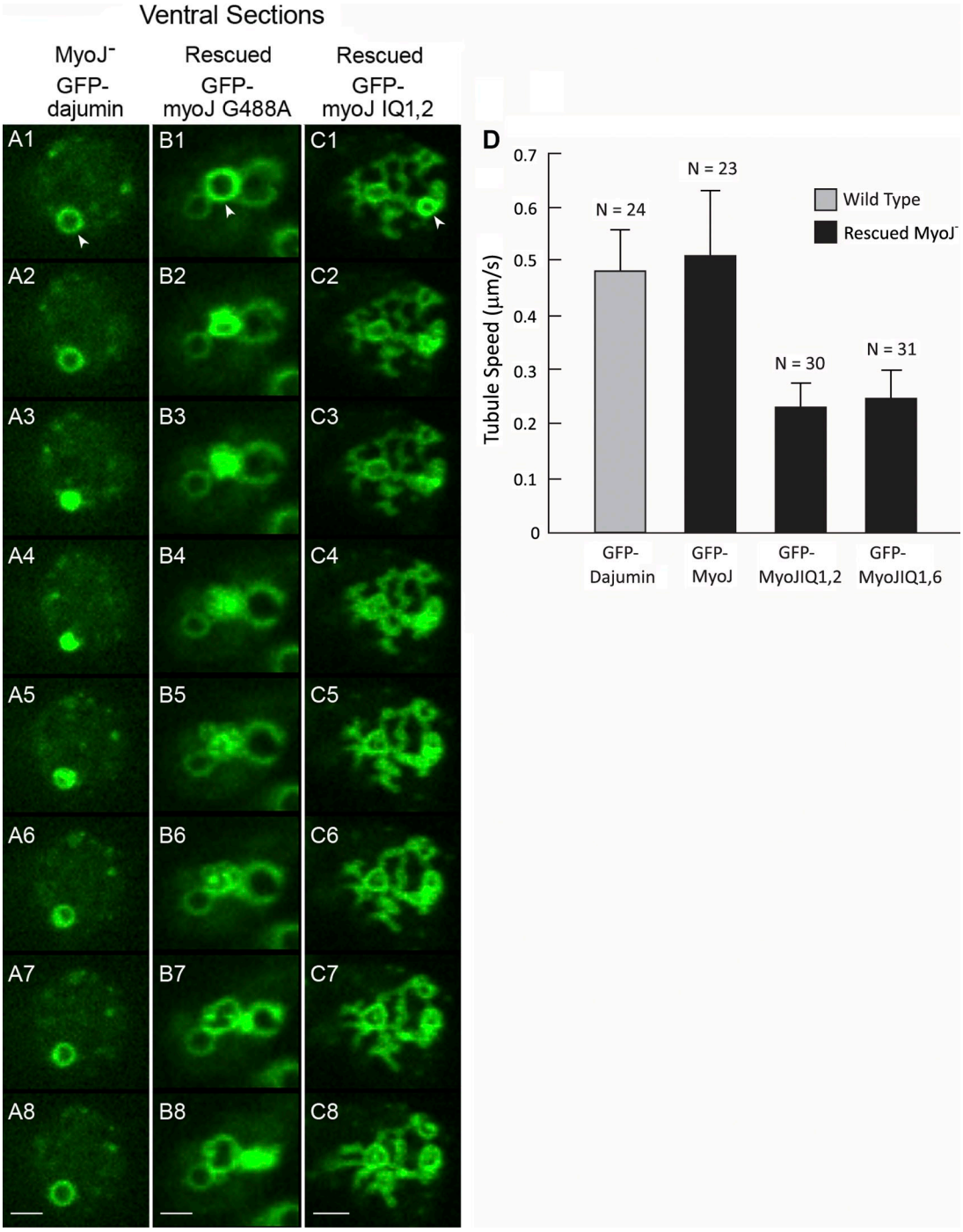

Figure 10. **Rescue with mechanochemically compromised versions of myoJ results in corresponding changes in CV membrane dynamics.** Shown are individual frames from the three movies presented in Video 8 that demonstrate the typical behavior at the ventral surface of CV bladders after water discharge in myoJ-null cells (bound using poly-lysine and imaged with GFP-dajumin) (A1–A8), myoJ-null cells complemented with GFP-myoJ G488A (B1–B8), and myoJ-null cells complemented with GFP-myoJ IQ1,2 (C1–C8). We note that we did not observe full fusion when myoJ-null cells were bound to poly-lysine–coated glass (Heuser, 2006), presumably because we used a lower concentration of poly-lysine. (D) Quantitative data for the speed of tubules moving along the cortex in the indicated strains. The values for null cells rescued with GFP-myoJ IQ1,2 or GFP-myoJ IQ1,6 were both significantly different from both controls (WT cells imaged with GFP-dajumin and null cells rescued with GFP-myoJ) ($P < 0.001$ in every pairing; Mann-Whitney). Bars: (A8, B8, and C8) 2 µm.

versions of myo2p containing progressively shorter lever arms (made by removing two, four, or six of myo2p's six IQ domains). Based on numerous studies of type V myosins in vitro, this in vivo effect presumably reflects a progressive reduction in myo2p's step size as its lever arm is progressively shortened (Sellers and Veigel, 2006). Therefore, we complemented myoJ-null cells with GFP-myoJ-1,2 IQ, a version of myoJ that contains only two of the myosin's six IQ domains (the first two). Imaging the ventral surface of complemented cells showed that this myosin rescued the association of CV membranes with the

cortex, as all 36 cells examined contained numerous CV bladders attached to the ventral surface (Fig. 10, C1–C8; Video 8, right movie). Moreover, when these bladders underwent discharge, the conversion of the membrane into radiating tubules was observed (Fig. 10, C1–C8; note that when the bladder marked by the arrowhead in frame C1 undergoes collapse in frame C5, short tubules can be seen to emanate from the collapsed membrane in frames C6-C8; Video 8, right movie). Although tubule appearance was restored in myoJ-null cells rescued with GFP-myoJ-1,2 IQ, the size and persistence of the tubules in these cells appeared to be significantly diminished relative to null cells complemented with WT GFP-myoJ (compare Video 8, right movie, to Video 7, left movie). Most importantly, the speed of the tubules in null cells complemented with GFP-myoJ-1,2 IQ (0.23 ± 0.05 μm/s; $n = 30$) was 48% that of null cells complemented with WT GFP-myoJ (Fig. 10 D). Essentially identical results were obtained when myoJ-null cells were complemented with GFP-myoJ-1,6 IQ, a second version of myoJ containing only two of its six IQ domains (in this case, the first and sixth ones) (Fig. 10 D). These results provide very strong evidence that myoJ is responsible for the extension and radiating movement of CV tubules along the actin cortex.

Discussion

We identified two major roles for myoJ in CV complex function in *Dictyostelium*. First, myoJ is required for the normal steady-state distribution of CV membranes in the actin-rich cortex. Second, myoJ drives the actin-based cortical motility of CV membrane tubules that arise from collapsed bladder membranes after water discharge and that then fill and fuse to assemble new CV bladders. Our confidence in assigning this latter role stems not only from the phenotype of myoJ-null cells, where the conversion of collapsed bladder membranes into outwardly radiating tubules does not occur, but also from the demonstration that complementation of myoJ-null cells with versions of myoJ possessing altered mechanochemical properties leads to corresponding alterations in the dynamics of these CV membrane tubules. Our results represent, therefore, an example of a type V myosin acting in a "conventional" fashion as a point-to-point membrane translocator (Woolner and Bement, 2009).

Our data do not support a role for myoJ in the contraction of the CV bladder during water discharge. Specifically, when bladders in myoJ-null cells do undergo discharge, the contraction of the bladder appears normal. Rather, CV bladder collapse in *Dictyostelium* may require a type I myosin, as antibodies against myosin IC block bladder collapse in *Acanthamoeba* (Doberstein et al., 1993). An alternative to actomyosin I–dependent contraction as the mechanism driving bladder collapse has been proposed (Heuser, 2006) in which the physical strain on the CV membrane when the bladder is fully extended, coupled with a natural tendency for CV membranes to tubulate (due to an asymmetry in the phospholipids that comprise the membranes) forms the driving force for contractile vacuole "contraction". This explanation seems quite plausible and, unlike a myosin-dependent contraction mechanism, is consistent with the fact that, in EM images, CV bladders are universally devoid of F-actin (Heuser et al., 1993). Interestingly, two F-BAR containing proteins appear to drive the tubulation of collapsed bladder membranes in *Dictyostelium* (Heath and Insall, 2008). Given this finding, and the likelihood that these two proteins remain active in myoJ-null cells, we speculate that bladder membranes in myoJ-null cells still convert to some extent into tubules upon bladder collapse, but that these tubules remain below the limit of detection in the light microscope. Only the subsequent action of myoJ to draw these tubules out across the actin-rich cortex makes them clearly visible.

How is the cortical F-actin that surrounds the site of bladder collapse consistently organized so that myoJ, a barbed end–directed motor, always drives the movement of CV tubules away from the site of collapse and in a predominantly radial fashion? One way for the cell to solve this design issue would be to make the fusion pore an initiating/organizing site for the assembly of a radial array of F-actin where pointed ends are proximal to the pore and barbed ends are distal to the pore. Along these lines, we note that in the EM images of unroofed cells (Heuser et al., 1993), star-like patches of F-actin on the inner surface of the ventral PM are prominent. Perhaps the fusion pore resides in the center of these arrays. More recent EM images (Heuser, 2006) have also shown an annulus of actin filaments that appears to form on the plasma membrane at the base CV bladders at the moment of their discharge. The dense actin meshwork comprising these rings, which may also have been witnessed in living cells imaged using GFP-LimE-ΔC as an F-actin reporter (Bretschneider et al., 2004; Heuser, 2006), may be generated by the Arp2/3 complex given the presence of 70° actin branches (Heuser, 2006). Like mouse myosin V in vitro (Ali et al., 2007), myoJ can presumably navigate branched actin arrays. If the array surrounding the pore is polarized such that along most available paths the pointed end of a branched filament is more proximal to the pore than is its barbed end, the net result could well be what is seen for tubule movement in vivo: a path that is always somewhat convoluted but that also always results in the net translocation of the tubule away from the site of bladder collapse.

We also identified a new component of the CV complex cycle in *Dictyostelium*. Specifically, we showed that CV tubules and vesicles move not only along the actin cortex in the plane of the plasma membrane, but also bi-directionally between the cortex and the MTOC via plus and minus end–directed microtubule motors. Our appreciation for this microtubule-dependent component of the CV cycle arose from our efforts to define the nature of the CV membrane aggregate that appears in the center of myoJ-null cells. This effort led us to view CV membrane dynamics in the middle of the cell, a view that misses the dramatic cortical motility of CV membranes seen in ventral confocal sections, but catches CV membrane movements along microtubules stretching from the centrosome to the plasma membrane. This microtubule-dependent component persists in myoJ-null cells but cannot on its own drive the normal steady-state distribution of CV membranes in the cortex. This absolutely requires myoJ. We think that this microtubule-dependent component, together with a slight imbalance in favor of the minus end–directed motor and a tendency of CV membranes to aggregate

when released from the cortex upon loss of myoJ, is what drives the central accumulation of CV membranes seen in myoJ-null cells. Overall, our results indicate that myoJ cooperates with bi-directional, microtubule-dependent motors to drive the normal distribution and dynamics of CV membranes in *Dictyostelium*. This result parallels what we found previously for melanosomes in mouse melanocytes, where myosin Va cooperates with long-range, bi-directional, microtubule-dependent movements to drive the normal accumulation of melanosomes at dendritic tips (the Cooperative-Capture model; Wu et al. 1998). One difference, however, is that myoJ clearly moves CV membrane tubules on cortical actin as well as "capturing" them there. Relevant to this, recent work has shown that myoJ is a processive motor in vitro (Taft et al. 2008), so it appears to be well suited for supporting tubule motility in vivo. It will be interesting to see if other parallels exist between myoJ/CV membranes and myosin Va/melanosomes, such as a role for a Rab GTPase in recruiting myoJ to the CV membrane much like myosin Va is recruited to the melanosome membrane through a receptor complex containing Rab27a (Fukuda et al., 2002; Strom et al., 2002: Wu et al., 2002).

Materials and methods

Cell culture, reagents, and general methods

The thymidine auxotroph JH10 was maintained in HL5 media supplemented with 5 mg/ml thymidine, whereas myoJ-null cells lines were maintained in plain HL5 media. For live cell imaging, adhered cells were switched into 20 mM potassium phosphate buffer (pH 6.6) just before imaging. To deplete F-actin, cells were incubated in the presence of 10 µM cytochalasin A for 20 min before fixation. To depolymerize microtubules, cells were incubated in the presence of 8 µg/ml nocodazole for 15 min at room temperature before fixation. All reagents were purchased from Sigma-Aldrich. SDS-PAGE and ECL-based Western blotting were performed as described previously (Jung et al., 2001). The crude and purified anti-myoJ antibodies were used in Westerns at dilutions of 1:5,000 and 1:500, respectively. Purification of genomic DNA from *Dictyostelium* and Southern blotting were performed as described in Jung et al. (1996).

Antibodies

To prepare the antibody against myoJ, an EcoR1 fragment spanning myoJ heavy chain residues 1153–1299, which span a portion of the myosin's central coiled coil domain, was obtained by digesting the Bluescript clone "1.9 Xba" (Hammer and Jung, 1996) with EcoR1 and cloning the ~460-bp EcoR1 fragment obtained into pGEX-3X. The expression and purification of this GST fusion protein, and the subsequent immunization of the rabbit, were performed exactly as described previously (Jung et al., 2001). The crude anti-myoJ polyclonal antibody obtained was purified by repeated absorption against a nitrocellulose membrane charged with the whole cell extract from a myoJ-null cell line exactly as described previously (Jung et al., 1996). The purified antibody was used at a dilution of 1:30 for immunofluorescence staining. The polyclonal antibody against *Dictyostelium* γ-tubulin was a gift of Drs. U. Eueteneuer and R. Graf (University of Munich, Munich, Germany), and the monoclonal antibody against the *Dictyostelium* vacuolar H^+-ATPase (proton pump) was a gift of A. Fok (University of Hawaii, Honolulu, HI). Both of these monoclonal antibodies were used at a dilution of 1:200 for staining. The monoclonal antibodies against α-tubulin (clone DM1A; Sigma-Aldrich), calmodulin (clone 2D1; Sigma-Aldrich), and actin (1378996, clone C4; Boehringer Ingelheim) were all used at a dilution 1:200 for staining. Goat anti–mouse IgG secondary antibodies (FITC, #115-095-146; TRITC, #115-025-146; Jackson Immunoresearch Laboratories) and goat anti–rabbit IgG secondary antibodies (FITC, #F9887; TRITC, #T6778; Sigma-Aldrich) were used at a dilution of 1:200. A goat anti–rabbit IgG secondary antibody labeled with Alexa Fluor 568 (Invitrogen) was used in Fig. S2 at a dilution of 1:200. In separate tests, none of these secondary antibodies showed significant reactivity in the absence of primary antibody, or any cross-species reactivity.

Immunofluorescence light microscopy

Cells adhered to coverslips were fixed for 5 min in 99% methanol, 1% formaldehyde at −15°C and stained as described previously (Jung et al., 1996). Fixed samples were imaged on a confocal microscope (LSM 510; Carl Zeiss, Inc.) using a 63x Plan-Apo objective (except for one widefield image in Fig. 2 [see legend]). Unless stated otherwise, 1-µm confocal sections are shown. In a few indicated images, the cells were flattened by agar overlay before fixation as described in Jung et al. (2001).

Spinning disk confocal microscopy

Time-lapse images of living cells expressing GFP-dajumin or GFP-myoJ were obtained using a Nipkow spinning disk confocal head (PerkinElmer) attached to an inverted microscope (IX-81; Olympus). Cells were imaged in 20 mM potassium phosphate buffer (pH 6.6) at 21°C. Images were taken using a 63x Plan Apo objective (1.4 NA) at a frame rate of 1 frame per second (acquisition for 300 ms, shuttered for 700 ms). GFP was excited at 488 nm and fluorescence emission was collected using an LP 500-nm filter and fixed diameter pinholes, producing ~1-µm-thick sections. Images were captured using a cooled CCD camera (Orca-ER; Hamamatsu Photonics) at a bin size of 2 under conditions of minimal illumination (less than 10 µW at the back aperture). Image analyses were performed using MetaMorph software (MDS Analytical Technologies). To measure the speed of CV tubule movement along the actin-rich cortex, ventral confocal sections taken at 1 frame per second were analyzed frame by frame. A single number represents an event where the advancement of the leading tip of the tubule could be distinguished for at least four consecutive frames. The rate in µm/s was then calculated by dividing the total distance traveled by the duration of the event using the conversion factor of 0.22 µm/pixel. If advancement of the tubule was not observed for two or more consecutive frames, these frames were excluded when calculating the rate. This correction prevented an underestimate of the rate of translocation especially for cells expressing GFP-myoJ with a shortened lever arm, as the movement of CV tubules in these cells tended to pause more often than in cells expressing WT myoJ. Similar measurements were made to determine the rate of plus and minus end–directed microtubule-dependent movements in WT cells expressing GFP-dajumin, except that middle confocal sections were analyzed. To increase the frequency of observing bladder discharge in ventral confocal sections of myoJ-null cells, the cells were plated on glass treated with a 0.1-mg/ml solution of poly-lysine (300–400 kD).

Measurement of cell survival after hypo-osmotic stress

WT and myoJ-null cells were grown to mid log in HL5, pelleted, suspended in water at a concentration of 10^5 cells/ml (determined by triplicate measurements using a Coulter counter), and incubated for 0, 3, or 24 h at room temperature with gentle shaking. To quantify cell survival, cell suspensions at each time point were diluted 100-fold in 1 ml of live, mid-log *Klebsiella aerogenes* bacteria and plated on SM agar plates (250 µl/100 mm plate). After incubation at 20°C for several days, the number of cells that had survived incubation in water was determined by counting the number of plaques present in the bacterial lawn. Percent survival was calculated using as 100% the initial determination of cell number. We note that plaque diameter was the same for WT and myoJ-null cells, indicating that myoJ-null cells do not possess any obvious deficit in phagocytic capacity. To quantify the survival of clonal lines expressing the dominant-negative, GFP-GTD construct, cells were incubated as above for 0 and 3 h in water and counted in triplicate using an Auto T4 cellometer (Nexcelcom Bioscience). Cells were also stained with Trypan blue to identify dead cells that were still intact. Comparison of these two measurements indicated that both control and GFP-GTD–expressing cells must lyse soon after dying. Cell death was taken as the sum of the decrease in cell number over 3 h in water (due to cell lysis) plus the accumulation of the small number of intact, Trypan blue–positive cells. To estimate the change in the percentage of dim cells in the population of GFP-GTD clonal transformants over 3 h of incubation in water, the total cellular GFP fluorescence of 200 randomly chosen cells was measured at 0 h. Dim cells were classified as those that fell in the bottom 10% of the cellular fluorescence distribution (these cells are not green to the eye). The percentage of cells that exhibited this low level of fluorescence was then determined in 200 randomly chosen cells after 3 h of incubation in water.

Vector constructions

The GFP-tagged version of the transmembrane protein dajumin in plasmid pDEXH (Gabriel et al., 1999), as well as mRFPmars–α-tubulin (Fischer et al., 2004; referred to here as RFP-tubulin), were gifts of Drs. A. Muller-Taubenberger and G. Gerisch (Max-Planck Institute for Biochemistry, Martinsried,

Germany). The full-length myoJ heavy chain cDNA, which is releasable as a 6753-bp BglII–BamH1 fragment where the ATG immediately follows the BglII site and the TAA immediately precedes the BamHI site, was cloned as follows (note: except for the DNA fragments used to create the myoJ gene targeting vector [see below], all nucleotide numbering corresponds to the full-length myoJ cDNA, i.e., beginning at the ATG [nucleotide 1], ending at the stop codon [nucleotide 6741], and with the two intron sequences present in the genomic clone [Jung et al., 1996] deleted). First, the 3′ end of the myoJ heavy chain coding sequence beginning at nucleotide 2364 and ending at nucleotide 6741 (i.e., at the stop codon), and followed by a BamH1 site, was amplified by PCR off of genomic DNA and TA cloned, yielding clone pDTj29. Second, RT-PCR was used to amplify the 5′ 3137 nucleotides of the myoJ heavy chain coding sequence in such a way that the resulting clone (pDTj31) contains a BglII site immediately preceding the ATG. The inserts of both pDTj29 and pDTj31 were verified by sequencing both DNA strands and comparing the sequence obtained to that of the complete myoJ genomic clone. To create the full-length myoJ cDNA clone pDTj33, a unique BbsI site at nucleotide 2723 in the myoJ sequence was used to stitch portions of the inserts of clones pDTj29 and pDTj31 together. Specifically, a 4024-bp BbsI–BamHI fragment spanning the 3′ 4018 bp of the myoJ coding sequence was released from clone pDTj29 and cloned into pDTj31 that had previously been digested with BbsI and BamHI and purified away from the BbsI–BamHI fragment spanning nucleotides 2723 and 3137. Finally, to express the full-length myoJ heavy chain in *Dictyostelium* as a fusion to the C terminus of GFP, the complete myoJ heavy chain coding sequence was released from pDTj33 by digestion with BglII and BamHI and cloned in the correct orientation into plasmid pTX-GFP, a Ddp1-based, $G418_R$ expression plasmid where expression is driven by the actin 15 promoter (Levi et al., 2000).

To generate GFP-tagged myoJ containing the G488A point mutation, the 6753 bp BglII–Bam H1 fragment containing the full-length myoJ coding sequence was cloned into plasmid pSP72 (Promega) and digested with EcoRV and SacI. Of the three fragments generated (a 1198-bp EcoRV–SacI fragment [nucleotides 1461 to 2659], a 1202-bp SacI–SacI fragment [nucleotides 2659 to 3861], and a 6815-bp fragment with EcoRV and SacI ends that comprises the vector and the remainder of the myoJ cDNA), only the latter two were purified by electroelution. A new 1198-bp EcoRV–SacI fragment was then generated by PCR using Pfu polymerase (Stratagene), the WT myoJ cDNA as template, and a 5′ primer in which the glycine residue at position 488, which lies immediately 3′ of the EcoRV site, was changed to an alanine residue. The specific primers used were: 5′-AGTTCAGATATCTATGCTTTTGAATCGTTTGAAGTGAACGGGTTCGAACAGTTTTGC-3′ and 5′-GATATTGAACTCTATCCCTATGAGCTCTCC-3′. To reconstruct the full-length myoJ cDNA with the G488A mutation, this PCR product was digested with EcoRV and SacI and cloned back into the ~8 Kb EcoRV–SacI fragment containing the pSP72 vector and the remainder of the myoJ cDNA. The resulting plasmid was then digested with SacI, phosphatase treated, and ligated with the 1202-bp SacI–SacI fragment. After selection of a pSP72 clone in which the SacI fragment had inserted in the correct orientation, the full-length myoJ heavy chain cDNA was released from pSP72 by digestion with BglII and BamHI and inserted in plasmid pTX-GFP in the correct orientation as described above for the WT myoJ clone.

To generate the two versions of GFP-tagged myoJ in which only two of the myosin's six IQ motifs are present (GFP-myoJ-1,2 IQ and GFP-myoJ-1,6 IQ), we took advantage of two natural MscI sites (spanning nucleotides 2433–2881) that bracket myoJ's IQ domain (nucleotides 2470–2895). Before altering the IQ domain, we first had to introduce a silent mutation into the only other MscI site present in the myoJ cDNA (at nucleotide 1956). To accomplish this, we preformed site-directed mutagenesis using a QuikChange Site-Directed Mutagenesis kit (Stratagene), the wild-type 1198 bp EcoRV–SacI fragment referred to above as template, and the following primers: 5′-GATAAGTTCACTCAATCACCTGGTGGACATCCACAAGGTAATGGTGGTCC-3′ and the complementary primer. The altered 1198-bp EcoRV–SacI fragment obtained was then reintegrated into the full-length myoJ cDNA exactly as described above for the generation of the G488A point mutant. This full-length pSP72 clone was then digested with MscI and the wild-type MscI–MscI fragment spanning the IQ domain of myoJ (i.e., IQ domains one through six) replaced with versions of the IQ domain containing either the first two IQ domains (1,2 IQ) or the first and last IQ domains (1,6 IQ), both of which were synthesized de novo with MscI ends by Blue Heron Biotechnology. The 1,2 IQ fragment began at the 5′ MscI site (nucleotide 2433) and ended with an in-frame McsI site immediately after the last residue of the second IQ domain (residue 870, nucleotide 2613). The 1,6 IQ fragment contained the sequence between the 5′ MscI site (nucleotide 2433) and the last residue of the first IQ domain (residue 845, nucleotide 2538) followed by the sequence between the first residue of the sixth IQ domain (residue 942, nucleotide 2827) and the natural MscI site at nucleotide 2881. Full-length clones is which these synthesized MscI fragments had inserted in the correct orientation were released from pSP72 with BglII and BamHI and cloned into pTX-GFP in the correct orientation.

The targeting construct for disruption of the myoJ heavy chain gene via a double crossover, homologous recombination event in the thymidine auxotroph JH10 was built in Bluescript. First, a 5′ end, 542-bp fragment of the myoJ heavy chain gene spanning amino acid residues 426–606 (nucleotides 1482–2024 in the genomic myoJ sequence) was amplified off of the full myoJ clone as an XbaI–BamHI fragment by PCR using the following primers: 5′-GCTCTAGAGTGGTGACGGGTAAAGAGTCG-3′ and 5′-CGGGATCCGGTTACTTTACCAGCATAATG-3′. This fragment was then digested with XbaI and BamHI and cloned into Bluescript, creating plasmid KO-A. Second, a 3′ end, 1646-bp fragment of the myoJ heavy chain gene spanning residues 682–1230 (nucleotides 2250–3896) was amplified as a BamHI–EcoRI fragment by PCR using the following primers: 5′-CGGGATCCCAATTTTCAACATCACTTGCAAC-3′ and 5′-CGGAATTCCTCACTACCCAATTTCTCTGAGG-3′. This fragment was then digested with BamHI and EcoRI and cloned into plasmid KO-A, creating plasmid KO-B. Finally, plasmid KO-B was digested with BamHI, phosphatase treated, and ligated with the ~3.25-kb BamHI cassette containing the THY selectable marker. Plasmid KO-C, in which the THY cassette had integrated in the correct orientation, was then digested preparatively with SstI and EcoRI to release the complete, linear disruption fragment. This fragment was used for electroporation of JH10 after its purification away from Bluescript. The DNA probes used for Southern blot analyses of myoJ knockout cell lines (see Fig. 1) were generated as follows. The 202-bp Probe A, which corresponds to nucleotides 3899–4101 of the myoJ gene, and which should detect an increase in the size of the natural, 2652-bp EcoRI fragment (spanning nucleotides 1498–4111) to ~5.7 kb after a double crossover, gene replacement event (due to the addition of the 3.25-kb THY cassette and the loss of 220 bp of myoJ gene sequence), was created by PCR amplification using the following primers: 5′-GGAGGCAAAGAAACAAATCAATCAATTAGAAC-3′ and 5′-CATCTTCAACCGATTGTTTTGATTG-3′. The 220-bp Probe B, which corresponds to nucleotides 2028–2248 of the myoJ gene, and which spans most of the myoJ sequence between the 5′ and 3′ heavy chain fragments used to create the linear gene disruption construct (nucleotides 2025–2249, which should be lost from the genome in a double crossover, gene replacement event), was generated by PCR amplification using the following primers: 5′-GAAACTGATCAATTCCTTGACAAGAATAAGG-3′ and 5′-GAACCAACAGAAAGGAATTTCATTGACG-3′.

All clonal PCR products, SDM products, and de novo synthesized products were confirmed by sequencing of both DNA strands. All full-length, GFP-tagged versions of the myoJ heavy chain were verified by Western blot analyses using anti-GFP and anti-myoJ on extracts of cells expressing the clones. While pTX-GFP is in principal episomal, we found that it integrates into chromosomal DNA with high frequency. We therefore examined at least three independent clonal cell lines for targeting of myoJ to CV membranes and CV membrane dynamics. In each case (i.e., myoJ-null cells complemented with WT GFP-myoJ, GFP-myoJ-G488A, GFP-myoJ-1,2 IQ, or GFP-myoJ-1,6 IQ), the independent clones were qualitatively indistinguishable.

Cell transformation

For the generation of myoJ-null cells, ~20 μg of DNA was introduced into 800 μl of 10^8 cells by electroporation using a Gene Pulser (1 kV, 3 μF, 4 mm cuvette; Bio-Rad Laboratories). After electroporation, cells were diluted into 120 ml of straight HL5 medium, incubated with shaking for 12 h, and then plated into 96-well cell culture plates (200 μl/well). Wells that appeared to contain single colonies were harvested and subjected to a second round of purification by serial dilution as described previously (Jung et al., 1996) so as to ensure that cell lines were clonal. To create stable cell lines expressing GFP-dajumin or various versions of myoJ tagged with GFP, the same procedure was followed except that G418 was added to a final concentration of 12 μg/ml at the time of plating, and the stable lines obtained were maintained in this concentration of G418.

Online supplemental material

Video 1: CV membrane dynamics at the ventral surface of WT and myoJ-null cells. Video 2: CV membrane dynamics in the middle of WT cells. Video 3: CV membrane dynamics in the middle of a field of WT cells. Video 4: Movement of CV membranes along microtubules in a WT cell. Video 5:

CV membrane dynamics in the middle of myoJ-null cells and WT cells treated with cytochalasin or nocodazole. Video 6: Movement of CV membranes along microtubules in a myoJ-null cell. Video 7: CV membrane dynamics in myoJ-null cells expressing GFP-tagged myoJ. Video 8: CV membrane dynamics at the ventral surface of myoJ-null cells and myoJ-null cells expressing mechanochemically compromised versions of myoJ. Figure S1: Endogenous myoJ colocalizes extensively with CV membranes illuminated with GFP-dajumin. Figure S2: In the absence of myoJ or F-actin, CV membranes retract from the cortex and accumulate in the center of the cell. Figure S3: Microtubule depletion by NZ. Figure S4: NZ treatment causes a dramatic increase in the cortical association of CV membranes that is myoJ dependent. Online supplemental material is available at http://www.jcb.org/cgi/content/full/jcb.200810147/DC1.

We thank Xufeng Wu, Chris Combs, Bill Shin, John Heuser, Margaret Clarke, Annette Muller-Taubenberger, Chris Yengo, and Ed Korn for their contributions and advice.

M.A. Titus was supported by the National Science Foundation.

Submitted: 23 October 2008
Accepted: 27 July 2009

References

Ali, M.Y., E.B. Krementsova, G.G. Kennedy, R. Mahaffy, T.D. Pollard, K.M. Trybus, and D.M. Warshaw. 2007. Myosin Va maneuvers through actin intersections and diffuses along microtubules. *Proc. Natl. Acad. Sci. USA.* 104:4332–4336.

Bretschneider, T., S. Diez, K. Anderson, J. Heuser, M. Clarke, A. Müller-Taubenberger, J. Köhler, and G. Gerisch. 2004. Dynamic actin patterns and Arp2/3 assembly at the substrate-attached surface of motile cells. *Curr. Biol.* 14:1–10.

Clarke, M., and J. Heuser. 1997. Water and ion transport. *In Dictyostelium*: A Model System for Cell and Developmental Biology. Y. Maeda, K. Inouye, and I. Takeuchi, Editors. Universal Academy Press Inc., Tokyo. 75–91.

Clarke, M., J. Köhler, Q. Arana, T. Liu, J. Heuser, and G. Gerisch. 2002. Dynamics of the vacuolar H(+)-ATPase in the contractile vacuole complex and the endosomal pathway of *Dictyostelium* cells. *J. Cell Sci.* 115:2893–2905.

Doberstein, S.K., I.C. Baines, G. Wiegand, E.D. Korn, and T.D. Pollard. 1993. Inhibition of contractile vacuole function *in vivo* by antibodies against myosin-I. *Nature.* 365:841–843.

Fischer, M., I. Haase, E. Simmeth, G. Gerisch, and A. Müller-Taubenberger. 2004. A brilliant monomeric red fluorescent protein to visualize cytoskeleton dynamics in *Dictyostelium. FEBS Lett.* 577:227–232.

Fok, A.K., M. Clarke, L. Ma, and R.D. Allen. 1993. Vacuolar H(+)-ATPase of *Dictyostelium discoideum*. A monoclonal antibody study. *J. Cell Sci.* 106:1103–1113.

Fukuda, M., T.S. Kuroda, and K. Mikoshiba. 2002. Slac2-a/melanophilin, the missing link between Rab27 and myosin Va: implications of a tripartite protein complex for melanosome transport. *J. Biol. Chem.* 277:12432–12436.

Gabriel, D., U. Hacker, J. Köhler, A. Müller-Taubenberger, J.M. Schwartz, M. Westphal, and G. Gerisch. 1999. The contractile vacuole network of *Dictyostelium* as a distinct organelle: its dynamics visualized by a GFP marker protein. *J. Cell Sci.* 112:3995–4005.

Gerisch, G., J. Heuser, and M. Clarke. 2002. Tubular-vesicular transformation in the contractile vacuole system of *Dictyostelium. Cell Biol. Int.* 26:845–852.

Hammer, J.A. III, and G. Jung. 1996. The sequence of the *Dictyostelium myo* J heavy chain gene predicts a novel, dimeric, unconventional myosin with a heavy chain molecular mass of 258 kDa. *J. Biol. Chem.* 271:7120–7127.

Heath, R.J.W., and R.H. Insall. 2008. *Dictyostelium* MEGAPs: F-BAR domain proteins that regulate motility and membrane tubulation in contractile vacuoles. *J. Cell Sci.* 121:1054–1064.

Heuser, J. 2006. Evidence for recycling of contractile vacuole membrane during osmoregulation in *Dictyostelium* amoebae—a tribute to Günther Gerisch. *Eur. J. Cell Biol.* 85:859–871.

Heuser, J., Q. Zhu, and M. Clarke. 1993. Proton pumps populate the contractile vacuoles of *Dictyostelium* amoebae. *J. Cell Biol.* 121:1311–1327.

Jung, G., X. Wu, and J.A. Hammer III. 1996. *Dictyostelium* mutants lacking multiple classic myosin I isoforms reveal combinations of shared and distinct functions. *J. Cell Biol.* 133:305–323.

Jung, G., K. Remmert, X. Wu, J.M. Volosky, and J.A. Hammer III. 2001. The *Dictyostelium* CARMIL protein links capping protein and the Arp2/3 complex to type I myosins through their SH3 domains. *J. Cell Biol.* 153:1479–1497.

Kollmar, M. 2006. Thirteen is enough: the myosins of *Dictyostelium discoideum* and their light chains. *BMC Genomics.* 7:183.

Levi, S., M. Polyakov, and T.T. Egelhoff. 2000. Green fluorescent protein and epitope tag fusion vectors for *Dictyostelium discoideum. Plasmid.* 44:231–238.

Liu, T., and M. Clarke. 1996. The vacuolar proton pump of *Dictyostelium discoideum*: molecular cloning and analysis of the 100 kDa subunit. *J. Cell Sci.* 109:1041–1051.

Peterson, M.D., A.S. Urioste, and M.A. Titus. 1996. *Dictyostelium discoideum* myoJ: a member of a broadly defined myosin V class or a class XI unconventional myosin? *J. Muscle Res. Cell Motil.* 17:411–424.

Schott, D.H., R.N. Collins, and A. Bretscher. 2002. Secretory vesicle transport velocity in living cells depends on the myosin-V lever arm length. *J. Cell Biol.* 156:35–39.

Sellers, J.R., and C. Veigel. 2006. Walking with myosin V. *Curr. Opin. Cell Biol.* 18:68–73.

Strom, M., A.N. Hume, A.K. Tarafder, E. Barkagianni, and M.C. Seabra. 2002. A family of Rab27-binding proteins. Melanophilin links Rab27a and myosin Va function in melanosome transport. *J. Biol. Chem.* 277:25423–25430.

Taft, M.H., F.K. Hartmann, A. Rump, H. Keller, I. Chizhov, D.J. Manstein, and G. Tsiavaliaris. 2008. *Dictyostelium* myosin-5b is a conditional processive motor. *J. Biol. Chem.* 283:26902–26910.

Woolner, S., and W.M. Bement. 2009. Unconventional myosins acting unconventionally. *Trends Cell Biol.* 19:245–252.

Wu, X., B. Bowers, K. Rao, Q. Wei, and Hammer JA III. 1998. Visualization of melanosome dynamics within wild-type and *dilute* melanocytes suggests a paradigm for myosin V function in vivo. *J. Cell Biol.* 143:1899–1918.

Wu, X.S., K. Rao, H. Zhang, F. Wang, J.R. Sellers, L.E. Matesic, N.G. Copeland, N.A. Jenkins, and J.A. Hammer III. 2002. Identification of an organelle receptor for myosin-Va. *Nat. Cell Biol.* 4:271–278.

Yengo, C.M., E.M. De la Cruz, D. Safer, E.M. Ostap, and H.L. Sweeney. 2002. Kinetic characterization of the weak binding states of myosin V. *Biochemistry.* 41:8508–8517.

Zhu, Q., and M. Clarke. 1992. Association of calmodulin and an unconventional myosin with the contractile vacuole complex of *Dictyostelium discoideum. J. Cell Biol.* 118:347–358.